



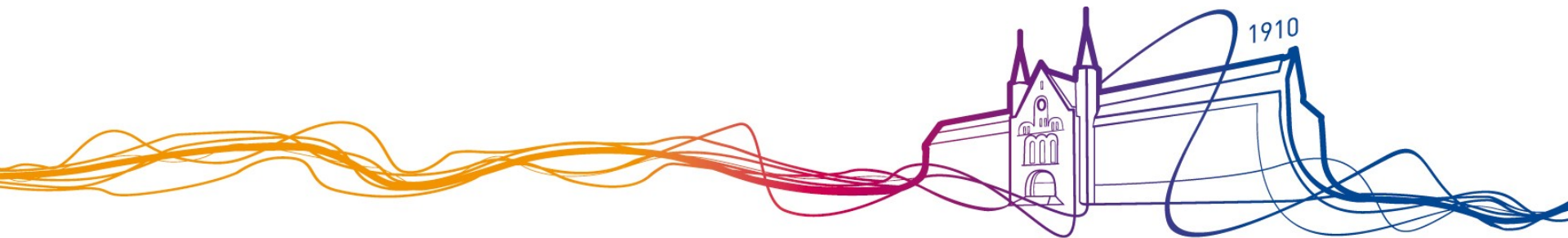
One-way wave-equation migration of compressional and converted waves in a VTI medium

Rose Meeting 2010

Ørjan Pedersen, IPT, NTNU

Bjørn Ursin, IPT, NTNU

Hans Kristian Helgesen, Statoil ASA



Contents

- Derive **phase-slowness expressions** for quasi-P and quasi-SV waves in a VTI medium which are used in a **one-way wave-equation migration** scheme.
- Numerical examples
 - demonstrate that the slowness approximations are valid for wide-angle propagation
 - the resulting one-way propagators are validated on a series of synthetic tests and applied on a field ocean-bottom seismic dataset.
- The results show that the method **accurately** images both compressional and converted waves in OBS data over a vertically transverse isotropic medium.

Wave characteristics

- The **characteristics of wave-propagation** can be described by the **dispersion relation**, relating the vertical (q) and horizontal phase-slowness (p).
- It can be found by combining the **stiffness coefficients** for a VTI medium with the **Christoffel-equation**.
- In a VTI medium

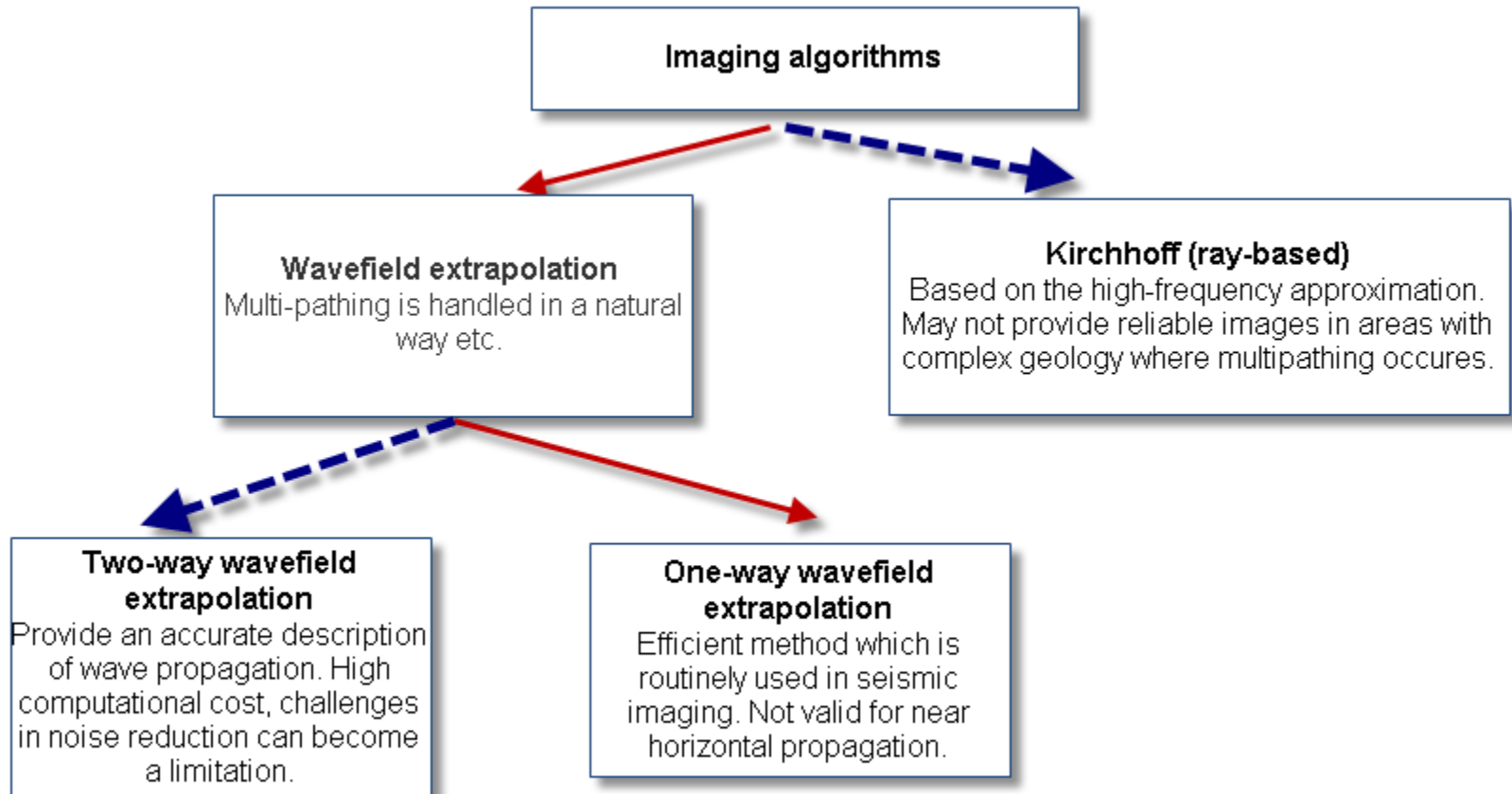
$$q_{\alpha,\beta}^2 = \frac{1}{2} (q_{\alpha_0}^2 + q_{\beta_0}^2 - 2p^2 (\sigma + \delta)) \mp \frac{1}{2} \left[(q_{\beta_0}^2 - q_{\alpha_0}^2)^2 - 4 \frac{p^2}{\alpha_0^2} (\gamma_0^2 - 1) (\sigma - \delta) + 4p^4 \left(2 \frac{(\gamma_0^2 - 1)}{\gamma_0^2} \sigma + (\sigma + \delta)^2 \right) \right]^{\frac{1}{2}},$$

$$\gamma_0 = \frac{\alpha_0}{\beta_0}, \quad q_{\alpha_0}^2 = 1/\alpha_0^2 - p^2$$

$$\zeta = \varepsilon - \delta, \quad q_{\beta_0}^2 = 1/\beta_0^2 - p^2$$

$$\sigma = \gamma_0^2 \zeta,$$

Main imaging methods



One-way wavefield extrapolation

- Given a wavefield $\Psi(z, :)$ at z
- Dividing the medium into layers of thickness Δz , the solution of the one-way wave-equation gives:

$$\Psi(z + \Delta z, :) = e^{\pm i\Delta z \omega q(p, x)} \Psi(z, :) \quad (1)$$

- Extrapolating the wavefield using (1) is expensive.
- Various approximative methods exist
 - Generalized Screen, Beamlets, Fourier finite-difference (FFD), etc.
 - Here, we focus on the FFD approach.
- FFD provide good accuracy vs. efficiency.

One-way wave field extrapolation

- For the FFD propagators, the propagator is separated into a phase-shift propagator in a constant background medium and a spatial finite-difference correction accounting for the varying model components.

$$q_{\alpha,\beta}(p, x) = q_{\alpha,\beta}^0(p) + \Delta q_{\alpha,\beta}(p, x)$$

Constant background Medium perturbations

- For the medium perturbations, we need to decouple the spatial and slowness components.
- Represent the phase-slowness as:

$$q_{\alpha,\beta} = \sum_{j \geq 0} k_j^{\alpha,\beta}(x) l_j^{\alpha,\beta}(p)$$
$$e^{i\omega \Delta z q_{\alpha}(p, x)} \approx \underbrace{e^{i\omega \Delta z q_{\alpha}^0(p)}}_{\text{Phase-shift}} \underbrace{e^{i\omega \Delta z \Delta q_{\alpha}(p, x)}}_{\text{Finite-difference term}}$$

Phase-slowness approximations

Exact expression:

$$q_{\alpha,\beta}^2 = \frac{1}{2} (q_{\alpha_0}^2 + q_{\beta_0}^2 - 2p^2 (\sigma + \delta)) \mp \frac{1}{2} \left[(q_{\beta_0}^2 - q_{\alpha_0}^2)^2 - 4 \frac{p^2}{\alpha_0^2} (\gamma_0^2 - 1) (\sigma - \delta) + 4p^4 \left(2 \frac{(\gamma_0^2 - 1)}{\gamma_0^2} \sigma + (\sigma + \delta)^2 \right) \right]^{\frac{1}{2}}$$

Series representation of square root (similar for q_β) yield:

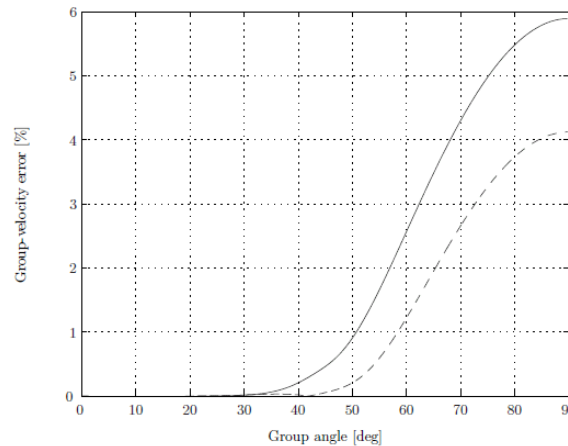
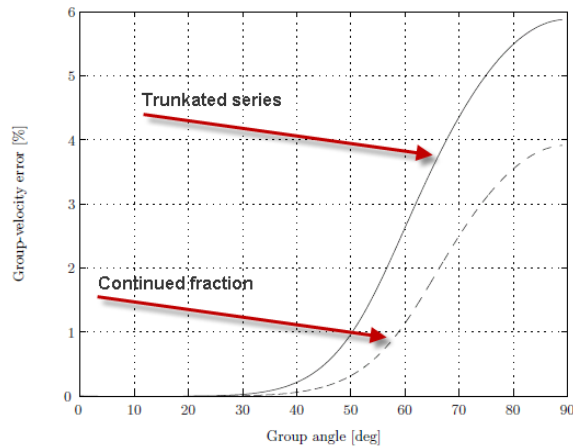
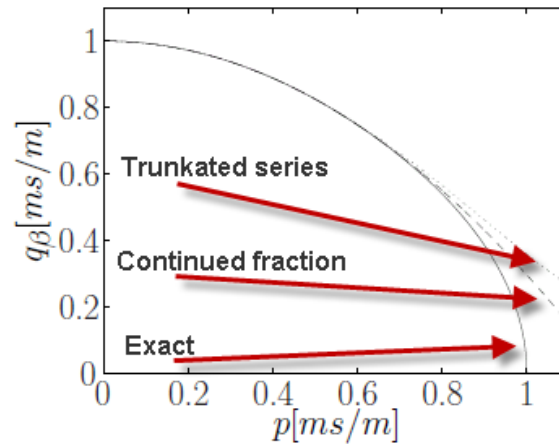
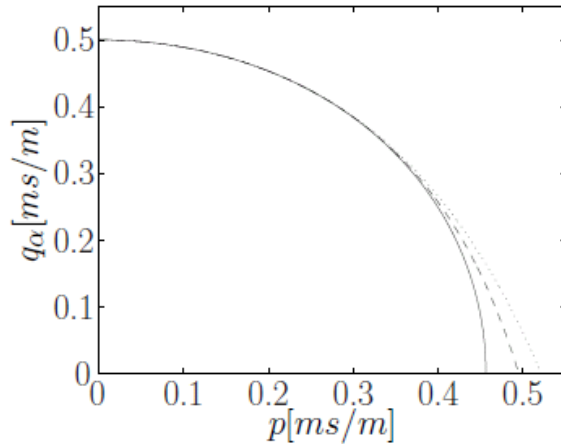
$$q_\alpha^2 = \frac{1}{\alpha_0^2} \left(1 - \sum_{j \geq 0} a_j (p\alpha_0)^{2j+2} \right)$$

We approximate the square-root by

$$q_\alpha = \frac{1}{\alpha_0} \left(1 - \sum_{j \geq 0} \tilde{a}_j (p\alpha_0)^{2j+2} \right) \quad (\text{Truncated series, } j=2)$$

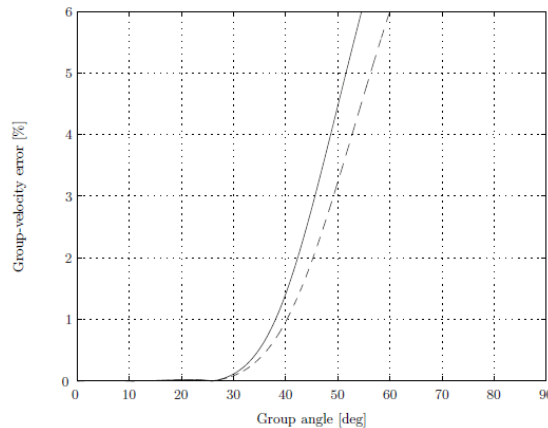
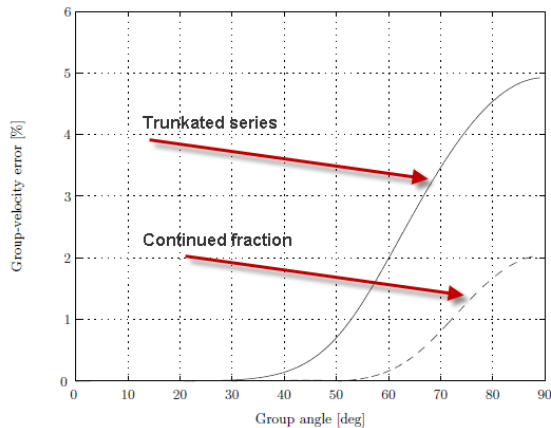
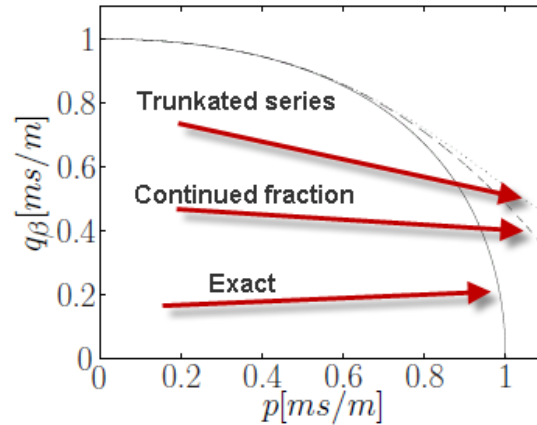
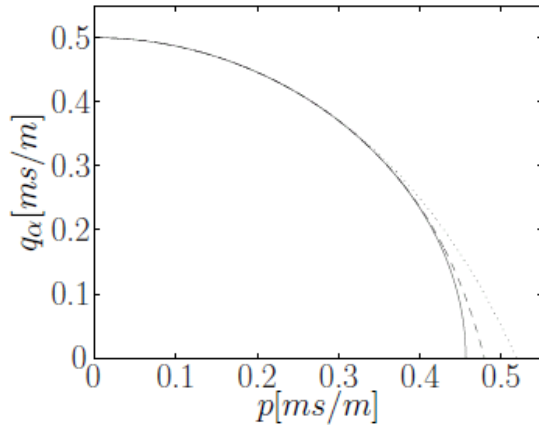
$$q_\alpha = \frac{1}{\alpha_0} \left(1 + \kappa_2^\alpha p^2 + \frac{\kappa_1^\alpha p^2}{1 - \kappa_0^\alpha p^2} \right) \quad (\text{Continuous fraction})$$

Accuracy of approximated slowness



- Medium parameters:
 $\alpha_0=2000\text{m/s}$
 $\beta_0=1000\text{m/s}$
 $\delta_0=0.05, \epsilon_0=0.10$
- Quantify accuracy of slowness approximations by looking at the corresponding relative error in group velocity (group angle).
- Less than 1% error:
 - $qP/qSV \sim 60^\circ$

Accuracy of approximate slowness



- Medium parameters:
 $\alpha_0=2000\text{m/s}$,
 $\beta_0=1000\text{m/s}$
 $\delta_0=0.15, \epsilon_0=0.10$
- Less than 1% error:
 - $qP \sim 70^\circ$
 - $qSV \sim 40^\circ$

One-way wave field extrapolation

$$e^{i\omega\Delta z q_\alpha(p,x)} \approx e^{i\omega\Delta z q_\alpha^0(p)} e^{i\omega\Delta z \Delta q_\alpha(p,x)}$$

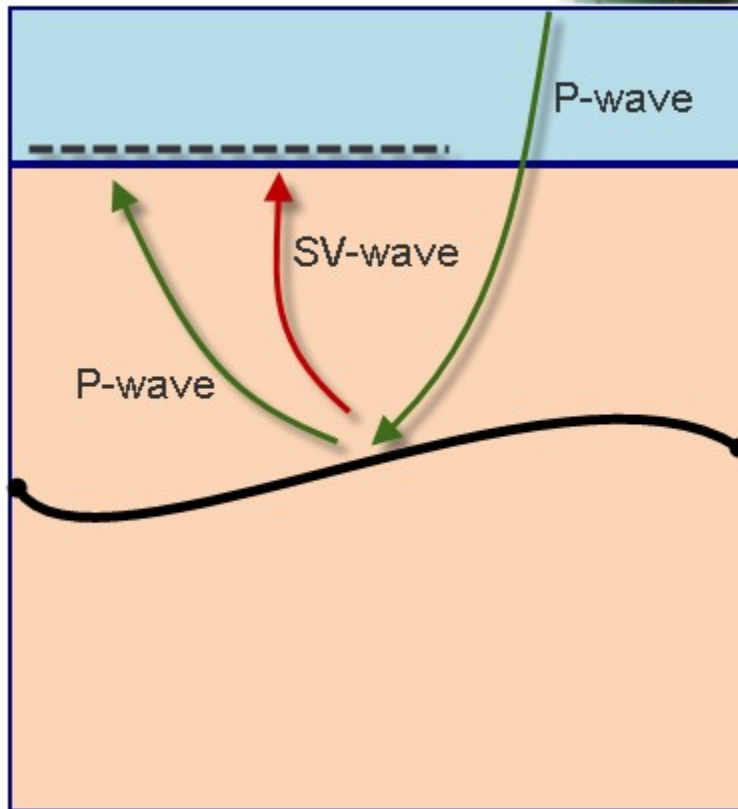
$$\Delta q_\alpha = q_\alpha - q_\alpha^0$$

$$= \frac{1}{\alpha_0} (1 - r) - \sum_{j \geq 0} (\tilde{a}_j - \tilde{a}_j^0 r^{2j+2}) (\alpha_0 p)^{2j+2}$$

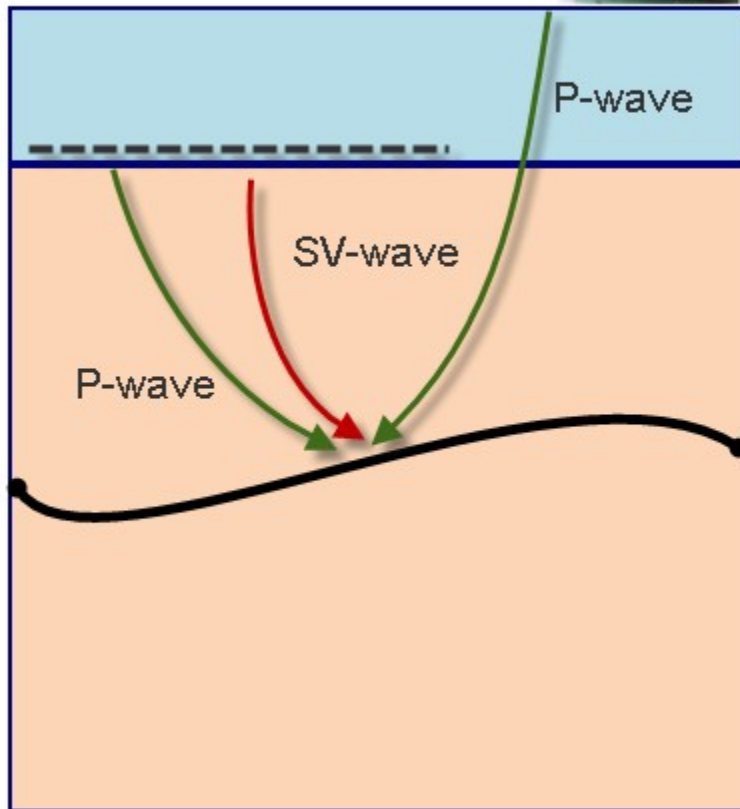
$$r = \alpha_0^0 / \alpha_0$$

$$\Delta q_\alpha \approx \frac{1}{\alpha_0} (1 - r) + \Delta \kappa_2^\alpha p^2 + \frac{\Delta \kappa_1^\alpha p^2}{1 - \Delta \kappa_0^\alpha p^2}$$

Ocean bottom seismic experiment



Ocean bottom seismic imaging



Wave field extrapolation:

$$D^{qP}(z + \Delta z, :) = e^{i\omega \Delta z q_\alpha(p,x)} D^{qP}(z, :)$$

$$U^{qP}(z + \Delta z, :) = e^{-i\omega \Delta z q_\alpha(p,x)} U^{qP}(z, :)$$

$$U^{qSV}(z + \Delta z, :) = e^{-i\omega \Delta z q_\beta(p,x)} U^{qSV}(z, :)$$

Imaging condition:

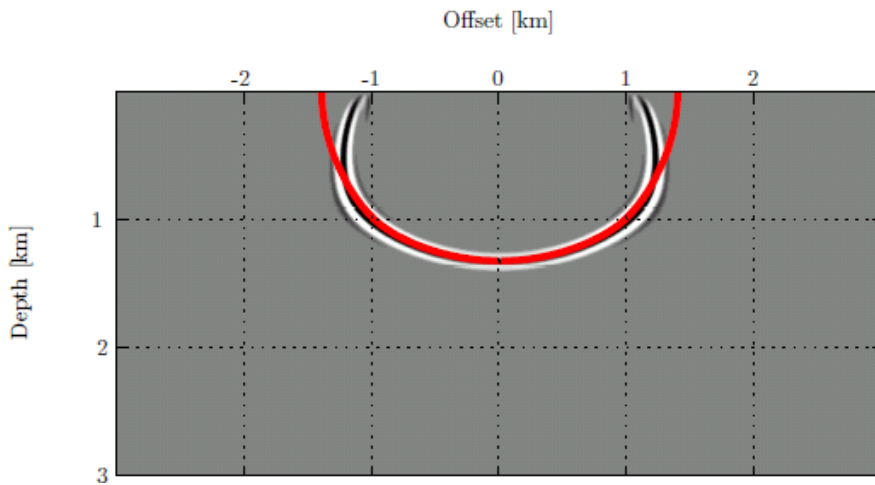
$$I^{qP,qSV}(z, :) = \sum_k \sum_\omega U_k^{qSV}(z, :) D_k^{qP}(z, :)^*$$

$$I^{qP,qP}(z, :) = \sum_k \sum_\omega U_k^{qP}(z, :) D_k^{qP}(z, :)^*$$

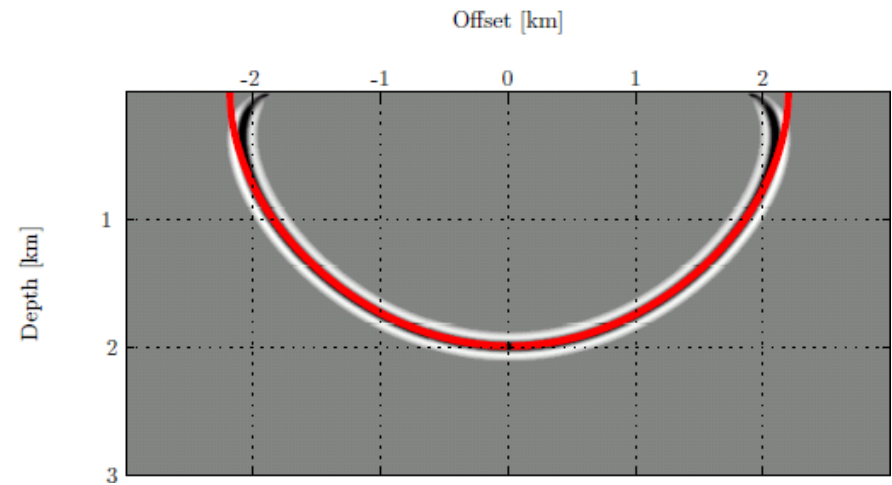
k common shot/receiver

Impulse response tests

The impulse response test involves migrating a single input seismic trace in a given medium. The input trace contains a single spike located at time 2.0 s



C-wave impulse



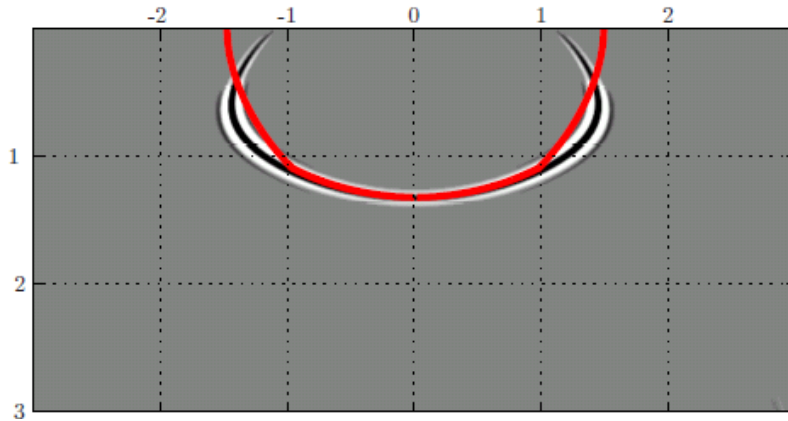
P-wave impulse

- Medium parameters: $\alpha_0 = 2000.0 \text{ m/s}$ $\beta_0 = 1000.0 \text{ m/s}$ $\alpha_0^0 = 1000.0 \text{ m/s}$; $\beta_0^0 = 750.0 \text{ m/s}$
 $\delta^0 = \delta = 0.0$ $\varepsilon^0 = \varepsilon = 0.1$
- By inspection, C-wave accurate up to about 50° , P-wave accurate up to about 70°
- For larger angles the error introduced by the medium perturbations cause the impulse response to be mis-positioned (inaccuracy of the qSV slowness approximation for large angles)

Impulse response tests

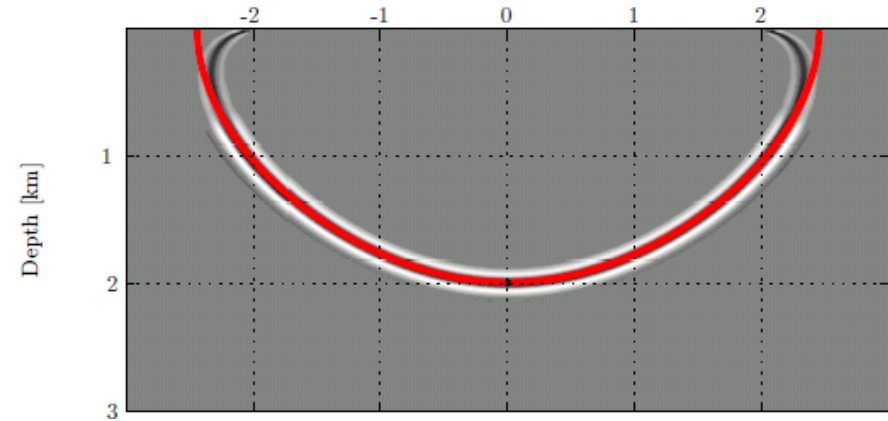
The impulse response test involves migrating a single input seismic trace in a given medium. The input trace contains a single spike located at time 2.0 s

Offset [km]



C-wave impulse

Offset [km]

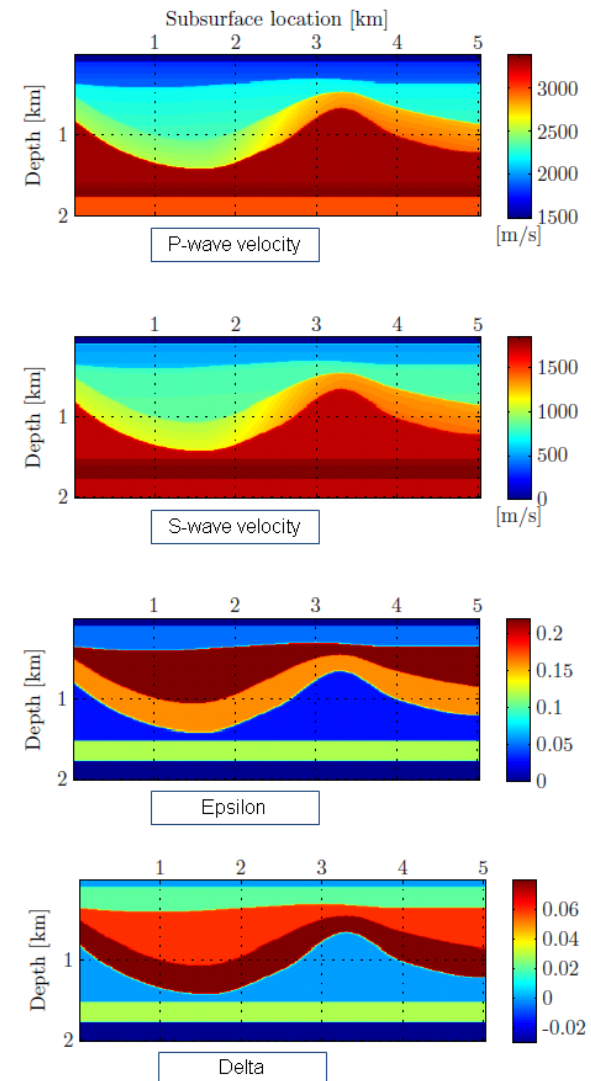


P-wave impulse

- Medium parameters: $\alpha_0 = 2000.0 \text{ m/s}$ $\beta_0 = 1000.0 \text{ m/s}$ $\alpha_0^0 = 1000.0 \text{ m/s}$ $\beta_0^0 = 750.0 \text{ m/s}$
 $\delta^0 = \delta = 0.05$ $\varepsilon^0 = \varepsilon = 0.25$
- By inspection, C-wave accurate up to about 45° , P-wave accurate up to about 70°
- In general, the accuracy of the derived one-way propagators for high dips depends on the variation of the medium properties.

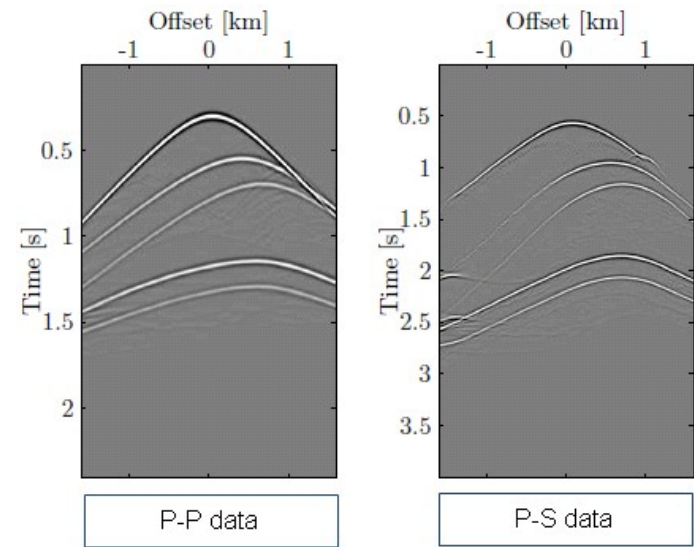
2D Synthetic data example

- We test the ability of the derived migration scheme to handle a subsurface with a relative high degree of medium perturbations.
- The model consists of 5 reflecting interfaces - the response from the sea-floor is not modelled.
- The receivers are placed at the sea-floor and the sources at the sea-surface.



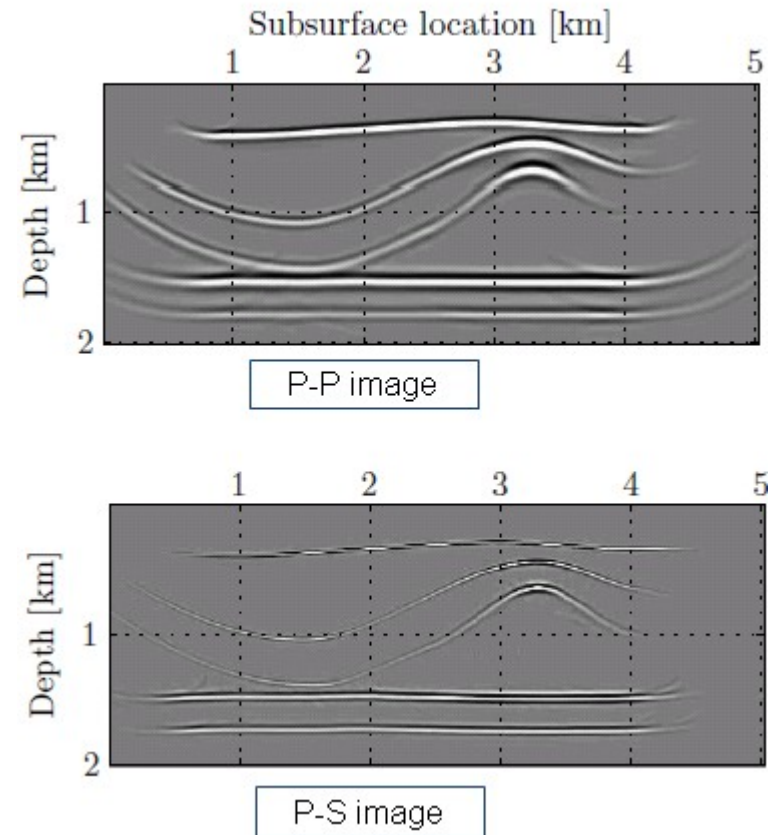
2D Synthetic data example

- A synthetic common-shot dataset was produced using a Born-Kirchhoff-Helmholtz modelling scheme (Ursin and Tygel, 1997) both for P-P and P-S waves.



2D Synthetic data example

- A synthetic common-shot dataset was produced using a Born-Kirchhoff-Helmholtz modelling scheme (Ursin and Tygel, 1997) both for P–P and P–S waves.
- After imaging, we see that both the C-wave and pressure-wave migration provide accurate results. The difference between the migrated sections is not very distinct, and the reflector interpretation would most likely coincide for both sections.
- Notice that the migrated P–S image has higher resolution than the migrated P–P image since the S-wave velocities are slower than the P-wave velocities.



3D Field data example - Volve

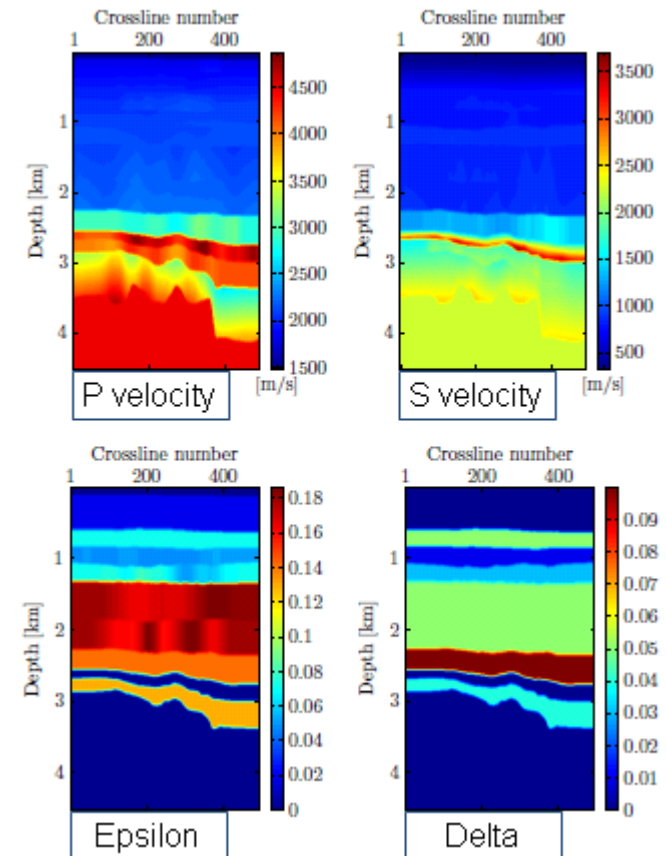
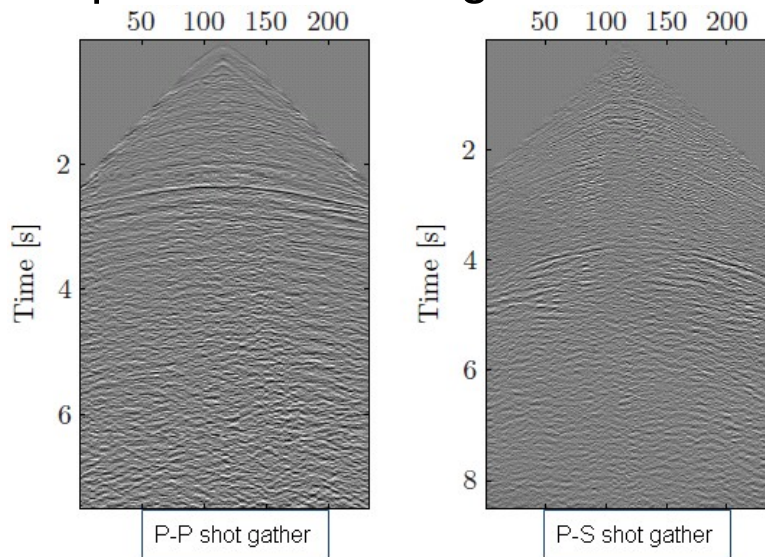
- We apply the derived one-way propagators on a 3D field OBS dataset. The OBS dataset was acquired in 2002 in the central North Sea over the Volve field. The field is located in the Sleipner area in the southern part of the Viking Graben.



Image from www.statoil.com

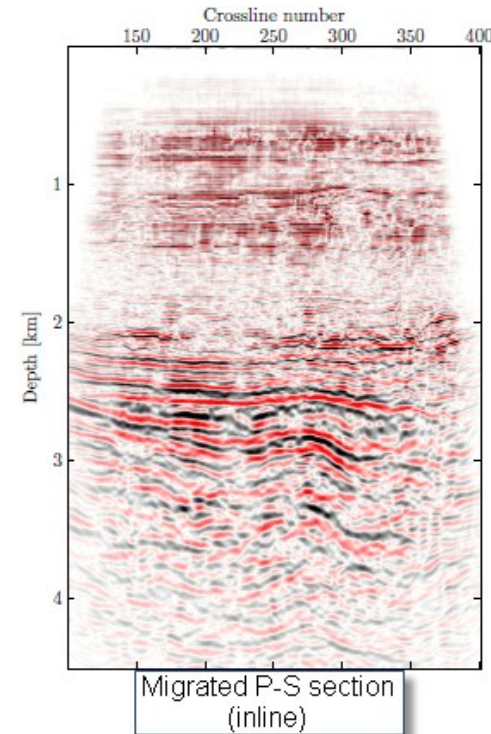
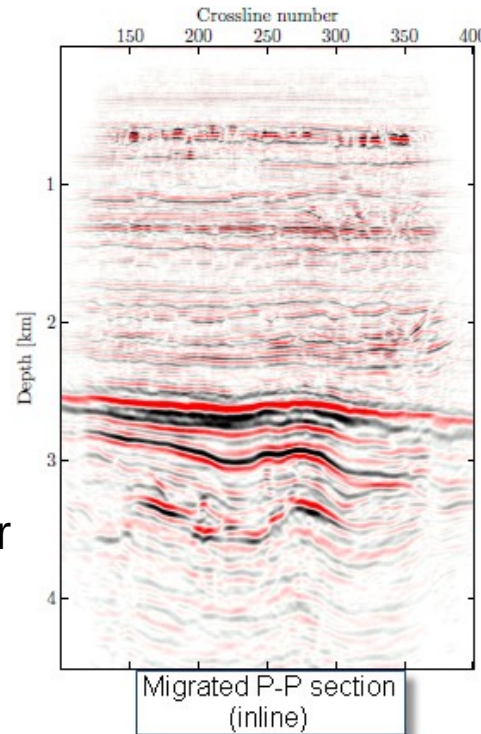
3D Field data example - Volve

- We apply the derived one-way propagators on a 3D field OBS dataset. The OBS dataset was acquired in 2002 in the central North Sea over the Volve field. The field is located in the Sleipner area in the southern part of the Viking Graben.



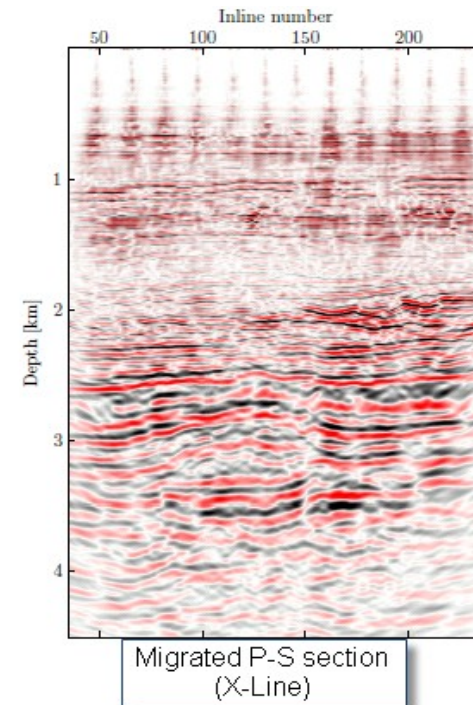
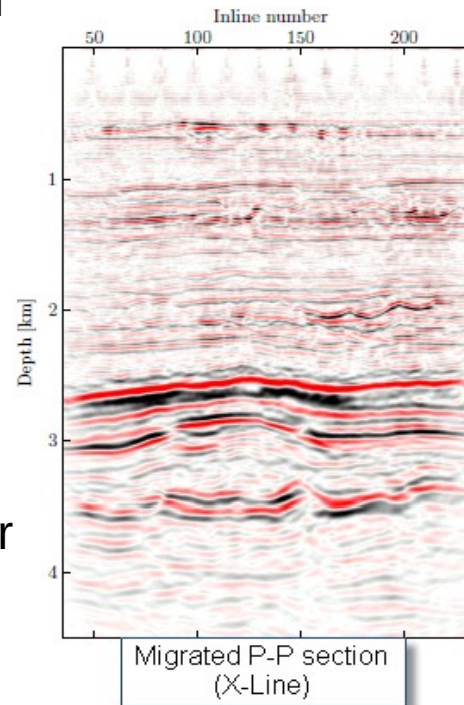
3D Field data example - Volve

- In general, the migrated images P–P and P–S show good structural focusing. The two images correlate well in depth.
- We notice that the migrated P–P image show better reflector continuity in the deeper part than the migrated P–S image and thereby seems to be better focused. Some differences are found between the distinction of some of the reflectors in the deeper part below about 3 km. These differences are most probably due to differences in the reflectivity for the converted waves.

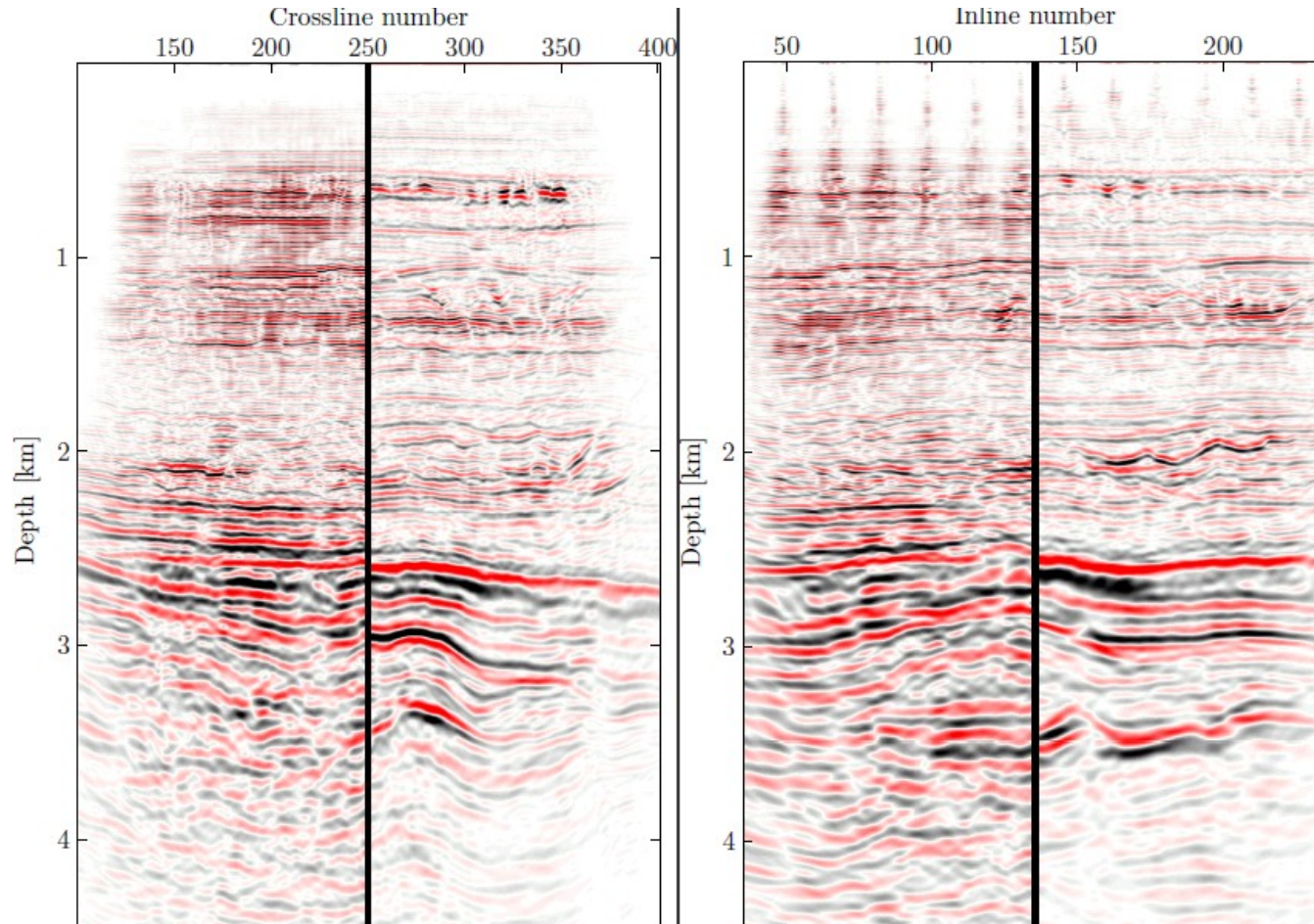


3D Field data example - Volve

- In general, the migrated images P–P and P–S show good structural focusing. The two images correlate well in depth.
- We notice that the migrated P–P image show better reflector continuity in the deeper part than the migrated P–S image and thereby seems to be better focused. Some differences are found between the distinction of some of the reflectors in the deeper part below about 3 km. These differences are most probably due to differences in the reflectivity for the converted waves.



3D Field data example - Volve



Conclusions

- We have developed a pre-stack migration scheme for compressional and converted waves using one-way propagators.
- The method builds on an FFD depth extrapolation scheme for which we derive approximations of the vertical qP and qSV slowness as a function of horizontal slowness p .
- By analysing the corresponding group-velocity as a function of group angle, we show that the approximations are accurate for high angles using small anisotropy parameters and weak non-hyperbolicity.
- Impulse responses demonstrate the propagator accuracy through good dip response and accurate kinematic behaviour for weak anisotropy. For higher values of the non-hyperbolicity parameter, the accuracy of the compressional propagators are still valid for high angles of propagation, while the C-wave propagators become more inaccurate.
- The 2D synthetic data example illustrates the methods ability to handle models with a realistic degree of laterally varying medium parameters. The data example also shows consistency between the compressional and C-wave images.
- The 3D field data example shows that the method is applicable to real data. Even though the compressional and C-wave images show differences in focusing and structural definitions, we also see good correlation in depth in the images.

Acknowledgement

- This research was supported by the Norwegian Research Council via the ROSE project.
- We would like to thank Statoil ASA for permission to publish and providing the field dataset.
- ØP would like to thank Joachim Mispel for help preparing the field data.
- Bjørn Ursin has received financial support from Statoil ASA through the VISTA project.